Pro-apoptotic BIM is an essential initiator of physiological endothelial cell death independent of regulation by FOXO3

Running Title: Role and regulation of BIM in endothelial death

Monica N. Koenig[1*], Edwina Naik[1,2,3*], Leona Rohrbeck[1,2], Marco J. Herold[1,2], Evelyn Trounson[1], Philippe Bouillet[1,2], Tim Thomas[1,2], Anne K. Voss[1,2], Andreas Strasser[1,2] and Leigh Coultas[1,2 #]

[1] The Walter and Eliza Hall Institute of Medical Research, 1G Royal Parade, Melbourne VIC 3052 Australia

[2] University of Melbourne, Department of Medical Biology, 1G Royal Parade, Melbourne, VIC 3052 Australia

[3] Current address: Genentech Inc, South San Francisco, CA 94080, USA

[*]These authors contributed equally to this work.

[#]Corresponding author:

Leigh Coultas
Development and Cancer Division
Walter and Eliza Hall Institute of Medical Research
1G Royal Parade, Parkville, Vic, 3052 Australia
Ph (+61) 3 9345 2860
Fax (+61) 3 9347 0852
Email: lcoultas@wehi.edu.au

Abstract:

The growth of new blood vessels by angiogenesis is essential for normal development but can also cause or contribute to the pathology of numerous diseases. Recent studies have shown that BIM, a pro-apoptotic BCL2-family protein, is required for endothelial cell apoptosis *in vivo*, and can contribute to the anti-angiogenic effect of VEGF-A inhibitors in certain tumour models. Despite its importance, the extent to which BIM is autonomously required for physiological endothelial apoptosis remains unknown and its regulation under such conditions is poorly defined. While the transcription factor FOXO3 has been proposed to induce *Bim* in response to growth factor withdrawal, evidence for this function is circumstantial. We report that apoptosis was reduced in $Bim^{-/-}$ primary endothelial cells, demonstrating a cell-autonomous role for BIM in endothelial death following serum and growth factor withdrawal. In conflict with *in vitro* studies, BIM-dependent endothelial death *in vivo* did not require FOXO3. Moreover, endothelial apoptosis proceeded normally in mice lacking FOXO-binding sites in the *Bim* promoter. *Bim* mRNA was up-regulated in endothelial cells starved of serum and growth factors and this was accompanied by the down-regulation of miRNAs of the *miR-17~92* cluster. *Bim* mRNA levels were also elevated in *miR-17~92*$^{+/-}$ endothelial cells cultured under steady state conditions, suggesting that *miR-17~92* cluster miRNAs may contribute to regulating overall *Bim* mRNA levels in endothelial cells.

Keywords:

Apoptosis/BCL2/blood vessel regression/BIM/hyaloid/miR-17~92

Abbreviations:

BIM, BCL2 interacting mediator of cell death; FOXO, forkhead box O; VEGF-A, vascular endothelial growth factor A; PI3K, phosphoinositide-3 kinase; BH3, BCL2-homology region 3; FACS, fluorescence activated cell sorting; PECAM1, platelet/endothelial cell adhesion molecule 1; QVD-OPH, quinoline-Val-Asp-CH_2-O-Ph.

Introduction

The growth of new blood vessels by angiogenesis is fundamentally important for matching vascular supply to the metabolic needs of growing tissues. While normally quiescent in adults, the angiogenic program can be re-activated in pathological form, facilitating the progression of numerous diseases including cancer, chronic inflammatory diseases, diabetic retinopathy and macular degeneration (1). Angiogenesis involves the proliferation, migration and differentiation of endothelial cells, followed by the remodelling of immature new vessels and the recruitment of peri-vascular support cells to form a mature vascular network. Vascular endothelial growth factor A (VEGF-A) is a pro-angiogenic cytokine essential for normal vascular development and angiogenesis (2) and is the major target for anti-angiogenic agents currently in clinical use (3). While such agents are effective in the treatment of intraocular vascular diseases (4), they have proven less effective against tumours, which display intrinsic and acquired resistance to VEGF-A inhibitors (5). The exact mechanism(s) by which VEGF-A inhibition prevents pathological vessel growth, particularly in the context of tumours, is the subject of debate. One effect of VEGF-A inhibition may be to impede endothelial cell survival: inhibition of VEGF-A signalling can trigger extensive endothelial cell apoptosis in both normal (6, 7), and tumour-associated vessels (8, 9), and exogenous VEGF-A can protect endothelial cells from apoptosis under conditions of stress such as in response to serum deprivation (10), and oxygen-induced retinopathy (OIR) (11). Understanding the molecular regulation of endothelial cell death may therefore provide useful information for the development of new agents for targeting pathological angiogenesis or the improvement of existing therapeutic strategies.

Apoptosis, or programmed cell death, is a genetically encoded program by which redundant and potentially harmful cells are eliminated from the body. Two pathways sense and transduce apoptotic signals: the intrinsic, BCL2 family-regulated pathway and the extrinsic, death receptor activated pathway. The BCL2 family of cell death regulators consists of both pro-survival and pro-apoptotic members (12). Apoptotic stimuli including cellular stresses such as growth factor withdrawal, loss of contact with support matrices (‘anoikis’) and DNA damage activate the ‘BH3-only’ subclass of pro-apoptotic proteins (BAD, BID, BIK, BIM, BMF, HRK, noxa and PUMA). BH3-only proteins bind and neutralize the pro-survival members of the family (BCL2, BCLX, BCLW, MCL1 and A1)

and either directly or indirectly trigger the activation of the multi-BH domain pro-apoptotic BCL2 family members BAK and BAX. Once unleashed, BAK and BAX cause the release of apoptogenic factors from the mitochondria including cytochrome C, ultimately resulting in the activation of cysteine proteases such as caspase-3, that cleave vital cellular constituents and activate DNases thereby demolishing the cell (12).

The BCL2-regulated pathway is essential for apoptosis regulation in endothelial cells. BCL2 expression in endothelial cells is induced by VEGF-A (13, 14), *Bcl2*$^{-/-}$ mice display increased endothelial apoptosis *in vivo* (15), whereas mice lacking both BAX and BAK display less (16). The BH3-only protein BIM plays a central role in the initiation of endothelial cell death and to date is the only BH3-only protein demonstrated to be necessary for this process (9, 17). VEGF-A has a key role in suppressing the activity of BIM: BIM is required for the apoptotic death of retinal endothelial cells during OIR (17), a process suppressed by ectopic VEGF-A (11), and BIM is required for the apoptotic death of tumour endothelial cells that occurs following VEGF-A inhibition (9). As BIM is required for apoptosis in a broad range of cell types (18), the use of germline *Bim* knockouts in these studies make it hard to separate its specific role in endothelial cells from possible indirect effects via other cell types. Furthermore, how any endothelial cell-autonomous activity of BIM might be regulated *in vivo* is not clear.

The PI3K/Akt pathway is important for endothelial cell survival including in response to the pro-angiogenic growth factors VEGF-A and angiopoietin-1 (Ang1) (10, 19), as well as blood flow shear stress (20). In the presence of growth factors, Akt promotes cell survival by phosphorylating the class O forkhead box (FOXO) transcription factors, leading to their expulsion from the nucleus, thus shutting down expression of their pro-apoptotic target genes (21). *Bim* is a direct transcriptional target of FOXO3 and is induced in response to cytokine deprivation (22-25). FOXO3 is expressed in endothelial cells and is repressed by PI3K/Akt signalling, including in response to VEGF-A *in vitro* (26, 27). While endothelial cells express multiple FOXO family members (26-28), *in vitro* studies implicate FOXO3 as the predominant regulator of *Bim* in this cell type: knockdown of *Foxo3* but not *Foxo1* resulted in reduced *Bim* expression in endothelial cells (27), whereas over-expression of constitutively active FOXO3 induced *Bim* expression (29). The requirement for FOXO3 in endothelial cell death in a physiologically relevant context however remains to be proven.

Here we present evidence that BIM is intrinsically responsible for the initiation of apoptosis in endothelial cells following serum and growth factor withdrawal. We show that BIM-dependent endothelial apoptosis *in vivo* proceeds normally in the absence of FOXO3, and does not require direct binding of FOXO factors to the *Bim* promoter. Up-regulation of *Bim* mRNA in endothelial cells following serum and growth factor withdrawal was accompanied by a corresponding reduction in miR-17-5p and miR-92a, miRNAs known to suppress BIM expression. Accordingly, *Bim* mRNA levels were elevated in *miR-17~92*$^{+/-}$ endothelial cells. Finally, through quantitative assessment of apoptosis using a range of endothelial cell death models, we show that, while BIM is an essential initiator of endothelial cell death in a range of circumstances, it is not the sole inducer of endothelial apoptosis.

Results

BIM is a cell-autonomous inducer of apoptosis in endothelial cells

We established a novel method for the culture of primary mouse endothelial cells to assess the cell-intrinsic role of BIM in endothelial cell death in the absence of other cell types. Endothelial cells were isolated from E9.5 embryos by FACS sorting based on expression of the endothelial markers PECAM1 and ICAM2 and lack of the hematopoietic markers CD45 and CD41 (PECAM1^{Hi} ICAM2^{Hi} CD45^{-} CD41^{-}). Sorted cells were plated on fibronectin and cultured for 3 days, after which time >97% of all cells expressed PECAM1 (Figure 1a). To assess the requirement of BIM for apoptosis in these cells, we sought to mimic conditions under which BIM is required for apoptosis *in vivo*. Given the known role for VEGF-A in repressing BIM-dependent endothelial cell death (9), we assessed viability in response to serum and growth factor deprivation as an approximation of VEGF-A withdrawal. Endothelial cells freshly isolated from *Bim*$^{-/-}$ and control (*Bim*$^{+/+}$ and *Bim*$^{+/-}$) littermate embryos were cultured for 3 days without passage, then deprived of serum and growth factors and viability monitored by time-lapse imaging over 36 h. Whereas endothelial cells from control embryos had undergone extensive apoptosis after 36 h of serum and growth factor deprivation, significantly less death was observed in *Bim*$^{-/-}$

endothelial cells from 21 h onward (Figure 1b). These results demonstrated a cell-autonomous requirement for BIM in endothelial cell death following withdrawal of serum and growth factors.

BIM is expressed in hyaloid endothelial cells and is required for hyaloid vessel regression

Having established that BIM acted autonomously to induce endothelial cell apoptosis, we sought to define how its activity was regulated in a physiological setting. Hyaloid vessels are a transient vessel network that services the developing eye prior to retina vascularization. In mice, these vessels begin to undergo apoptotic regression beginning at postnatal day (P) 5, resulting in a substantial reduction in vessel density by P8 and complete clearance by around P14. Hyaloid vessel regression requires the intrinsic apoptosis pathway as it is prevented in the combined absence of BAK and BAX (16). Hyaloid endothelial apoptosis is initiated by pericyte-derived Ang2, which blocks Ang1-dependent activation of Akt (30) and requires macrophage-derived WNT7b (30, 31). BIM has been implicated in hyaloid vessel regression (17), but its expression, the extent of its requirement, and its regulation in this system have not been determined.

In situ hybridization at P6 demonstrated that *Bim* mRNA was indeed expressed in hyaloid vessels during their active regression phase (Figure 2a). Using $Bim^{lacZ/+}$ mice (32), we found that in addition to endothelium, *Bim* was expressed in pericytes and ocular macrophages – cell types with active roles in hyaloid regression (Figure 2b) (30). Quantification of hyaloid vessels at P8 showed that $Bim^{-/-}$ pups contained significantly more hyaloid vessels than control littermates, demonstrating that BIM was indeed required for hyaloid vessel regression (Figure 3a). BIM deficiency afforded less protection than that reported in the absence of Ang2, WNT7b or ocular macrophages however (30, 31), and examples of apoptotic vessels were still observed in BIM-deficient mice (n = 5) (Figure 3b). Nonetheless, loss of BIM provided long-term protection from regression as those vessels that failed to regress during the neonatal period persisted into adulthood (Figure 3c). These results demonstrate that BIM is required for hyaloid vessel regression, but similar to the extent of its role in endothelial cells deprived of serum and growth factors, it is not solely responsible for apoptosis in this system.

Bim *mRNA is elevated in hyaloid endothelial cells undergoing regression*

Inhibition of VEGF-A *in vivo* leads to enhanced *Bim* gene transcription in endothelial cells (9). To determine whether *Bim* was regulated at the mRNA level during hyaloid regression, we compared *Bim* mRNA levels in regressing (P5) and non-regressing (P1) vessels. As our expression analysis showed that *Bim* was expressed in ocular macrophages and pericytes in addition to endothelial cells, we performed our analysis on FACS sorted hyaloid endothelial cells. Quantitative RT-PCR showed that *Bim* levels were 2.4 fold higher in hyaloid endothelial cells from P5 vessels compared to those at P1 (Figure 4a). This result demonstrated that *Bim* expression during hyaloid vessel regression was regulated at the mRNA level.

BIM-dependent hyaloid vessel regression occurs independently of FOXO3 or direct FOXO binding to the* Bim *promoter

As FOXO3 is a reported transcriptional regulator of *Bim*, we sought to determine whether it was required for BIM-dependent hyaloid vessel regression. Quantitative comparison of hyaloid vessel numbers in $Foxo3^{-/-}$ and $Foxo3^{+/+}$ littermates at P8 showed that hyaloid vessel regression proceeded normally in the absence of FOXO3, demonstrating that it was not required for endothelial apoptosis in this system (Figure 4b). FOXO1 and FOXO4 are two related family members to FOXO3 and bind the same consensus DNA sequence (33). FOXO1 & 4 are expressed in endothelial cells, where they are targets for repression by PI3K/Akt signalling (26-28). Semi-quantitative RT-PCR performed on FACS-sorted, P5 hyaloid endothelial cells showed that *Foxo1*, and to a lesser extent *Foxo4*, were more abundantly expressed in hyaloid endothelium than *Foxo3* (Figure 4c). To establish whether BIM-dependent hyaloid regression was due to the redundant activity of FOXO transcription factors, we assessed hyaloid vessel regression in mice in which the 4 FOXO binding sites located between positions -625 to +2,509 of the *Bim* transcriptional start site had been mutated ($Bim^{\Delta Foxo}$) (34). Mutation of these four binding sites prevents transcriptional induction of *Bim* by constitutively active FOXO3 (34). Quantitative assessment at P8 showed that hyaloid regression proceeded normally in $Bim^{\Delta Foxo/\Delta Foxo}$ mice (Figure 4d). Together these results demonstrate that BIM-dependent hyaloid vessel regression proceeds

independently of FOXO3, and does not require direct FOXO-dependent regulation of the *Bim* promoter.

BIM-dependent endothelial cell apoptosis during hypoxia-induced angiogenesis occurs independently of FOXO3 or direct FOXO binding to the* Bim *promoter

In light of the previous results, we investigated whether FOXO-dependent regulation of *Bim* was required for endothelial cell apoptosis in other physiologically relevant contexts. Endothelial apoptosis has been reported in retinal vessels at P5 (35), where it is thought to account for vessel pruning around arteries in response to local reductions in VEGF-A levels (36). We investigated whether endothelial apoptosis in the P5 retinal vasculature was affected in $Bim^{-/-}$, $Foxo3^{-/-}$ or $Bim^{\Delta Foxo/\Delta Foxo}$ mice by staining for activated caspase-3, then imaging the entire retinal vasculature by confocal microscopy and quantifying the total number of apoptotic endothelial cells in each eye. BIM-deficient mice showed a significant reduction in the number of apoptotic endothelial cells per retina at P5, indicating that BIM is required for much (but not all), of the apoptosis occurring in the angiogenic retinal vasculature at this time (Figure 5a). In contrast, $Foxo3^{-/-}$ and $Bim^{\Delta Foxo/\Delta Foxo}$ mice showed normal rates of endothelial apoptosis in the P5 retinal vasculature (Figure 5b and c). As for hyaloid vessel regression, these results demonstrate that physiological, BIM-dependent endothelial cell death *in vivo* occurs independently of FOXO3, and does not require direct regulation of the *Bim* promoter by FOXO transcription factors.

Elevated* Bim *mRNA in endothelial cells following serum and growth factor withdrawal is accompanied by reductions in miRNAs of the* miR-17~92 *cluster

The *miR-17~92* cluster is a well-established regulator of *Bim* expression at the post-transcriptional level (37-39). To determine whether *miR-17~92* miRNAs might contribute to regulating *Bim* mRNA levels in endothelial cells, we investigated the expression of two members of this cluster: miR-17 and miR-92a in endothelial cells 24 h after serum and growth factor withdrawal. Quantitative RT-PCR performed using TaqMan probes showed that *Bim* mRNA was strongly induced (~15 fold) in response to serum and growth factor deprivation (Figure 6a). In contrast, miR-17-5p was reduced by ~60% and miR-92a-3p more subtly by ~25% (Figure 6b), suggesting *Bim* mRNA levels in serum and growth factor

starved endothelial cells may be regulated at the post-transcriptional level by members of the *miR-17~92* cluster.

To validate a role for the miR-17~92 cluster in regulating *Bim* expression, we investigated *Bim* mRNA levels in endothelial cells cultured from E9.5 *miR-17~92*$^{+/-}$ embryos (37) by quantitative RT-PCR using TaqMan probes. miR-17~92 miRNAs are reduced by around 50% in *miR-17~92*$^{+/-}$ animals (37), therefore *miR-17~92*$^{+/-}$ endothelial cells are expected to contain comparable levels of mir-17~92 miRNAs to the cells starved of serum and growth factors described above. Under steady state conditions (unstarved), we found that *Bim* mRNA levels were elevated in *miR-17~92*$^{+/-}$ endothelial cells compared to littermate controls, consistent with a role for miR-17~92 miRNAs in repressing *Bim* mRNA levels at steady state (Figure 6c). In contrast, the effect of miR-17~92 cluster loss on *Bim* levels was not observed in endothelial cells that had been serum and growth factor-starved for 24 h (Figure 6c). It should be noted that the control group in this experiment was composed of the following genotypes: *miR-17~92*$^{flox/+}$without the cre-recombinase and *miR-17~92*$^{flox/+}$with the cre-recombinase present. In the latter case, the cre-recombinase was found to be inefficient, resulting in retention of the functional *miR-17~92*^{flox} allele in the majority of the cells. Therefore, these animals were classified as controls. In addition, all control animals had one wild type *miR-17~92*$^{+}$ allele. Animals displaying complete heterozygous deletion of the *miR-17~92* allele were classified as *miR-17~92*$^{+/-}$ embryos. *Bim* levels in endothelial cells of all the control animals were uniformly low. In contrast, complete heterozygous deletion of the *miR-17~92* allele resulted in a 3 fold increase in *Bim* mRNA above controls (Figure 6c).

Discussion

We have extended the range of cell types known to express *Bim* to include pericytes and tissue-specific macrophages. Both these cell types influence endothelial cell viability, and depending on the context may act to promote (30, 31, 35), or suppress apoptosis (40, 41) This reinforces the need to address the extent to which BIM acts cell-autonomously to promote endothelial cell apoptosis, independently of effects on other cell types that influence the vasculature. As BIM is essential for apoptosis in many hematopoietic cell types (42) and

many endothelial cell-specific *Cre* lines are highly active in hematopoietic cells (43, 44), we established an *in vitro* viability assay for primary mouse endothelial cells to formally assess the cell-intrinsic role of BIM in endothelial cell death in the absence of other cell types. While previous *in vitro* analysis of apoptosis in *Bim*$^{-/-}$ endothelial cells has implicated a cell-autonomous role for BIM, the use of immortalized cells and an extremely high dose of 5-fluorouracil (5 mM) as a death stimulus means these results may not reflect a physiologically relevant role for BIM in endothelial apoptosis (45). In contrast, we developed an assay using non-immortalized, un-passaged, primary endothelial cells and a death stimulus (serum and growth factor withdrawal), to verify that BIM is indeed autonomously required for endothelial cell apoptosis under conditions relevant to the known *in vivo* role of BIM downstream of VEGF-A (9).

Our detailed time-lapse imaging approach revealed that BIM was dispensable for endothelial cell apoptosis in the first 14 hours following serum starvation, during which time approximately 40% of endothelial apoptosis occurred. This may reflect a biphasic response of endothelial cells to serum and growth factor withdrawal, for which BIM is required only in the second phase. Alternatively, there may be heterogeneity among the endothelial cells in our culture, with only some requiring BIM to undergo apoptosis. Either way, this result implicates factors in addition to BIM for the initiation of apoptotic death in endothelial cells. Indeed, in none of the contexts we investigated was endothelial death initiated by BIM alone. We have yet to identify other BH3-only proteins that act in concert with BIM to elicit endothelial apoptosis. Potential candidates with known expression in endothelial cells *in vivo* include BIK in hyaloid endothelial cells (46), and PUMA in retinal endothelial cells (47). PUMA seems particularly attractive given its known role in serum and growth factor withdrawal-induced apoptosis in other cell types (48). Paradoxically however, it has been reported to play a pro-survival, pro-proliferative role in endothelial cells (47). Given that extensive tissue-specific redundancy exists among BH3-only proteins (49), endothelial cell death will likely depend on multiple BH3-only proteins. Therefore, complete blockade of the intrinsic apoptotic pathway in endothelial cells, for example through deletion of both BAK and BAX, will be required to determine the full extent to which this pathway is responsible for endothelial cell death.

Despite *in vitro* evidence that FOXO3 is sufficient to induce *Bim*-dependent apoptosis in endothelial cells (27, 29), we found no evidence that FOXO3 was required for BIM-dependent endothelial cell apoptosis *in vivo*. It has been reported that FOXO3 can induce BIM expression in endothelial cells independently of binding to the FOXO consensus sequence (29). While we can exclude an indirect role for FOXO3 in BIM-dependent endothelial apoptosis, we cannot exclude such a role for FOXO1 or FOXO4. The importance of FOXO1 and FOXO4 in *Bim*-dependent endothelial death is questionable, however. Unlike *Foxo3*, knockdown of *Foxo1* in endothelial cells did not affect levels of *Bim* (27), and while expression of constitutively active FOXO4 could induce *Bim* expression and apoptosis in endothelial progenitor cells, it did not induce death in mature endothelial cells (50). Taken in combination with recent findings in hematopoietic cells (34), it would appear that direct FOXO binding to the *Bim* promoter is not critical for BIM-dependent apoptosis in general. However our analysis of endothelial apoptosis was by no means exhaustive, and we cannot exclude the possibility that FOXO3-dependent *Bim* activity in endothelial cells will be required in specific circumstances for cell killing, for example in response to reactive oxygen species (51).

Given the central importance of BIM in both developmental and stress-induced endothelial cell death *in vivo*, it is important to resolve how its activity in these cells is regulated independent of FOXO3. A major component of miRNA-mediated post-transcriptional gene repression is through target mRNA degradation (52). *Bim* is a well-defined target of the miR-17~92 microRNA cluster (37, 38) and VEGF induces the expression of *miR-17~92* cluster members in endothelial cells (53). Our *in vitro* data have shown that up-regulation of *Bim* mRNA in response to serum and growth factor withdrawal is accompanied by a corresponding decline in the levels of *mir-17~92* cluster member miR-17-5p and to a lesser extent miR-92a-3p (~60% and ~25% respectively). Given our finding that *Bim* mRNA levels were elevated in *miR-17~92*$^{+/-}$ endothelial cells, and *mir-17~92*$^{+/-}$ animals express 50% less miR-17~92 miRNAs (37), the 60% reduction in miR-17-5p observed following serum and growth factor starvation would appear sufficient to promote an increase in *Bim* mRNA expression. The level of miR-92a reduction is less convincing in this regard. Levels of other miR-17~92 cluster members following serum and growth factor starvation were not investigated. The lack of effect of *mir-17~92* heterozygosity on *Bim*

levels following 24 h of serum and growth factor starvation is likely due to the advanced stage of cell death commitment at this time point (70% of cells are normally dead by 24 h), and maximal induction of *Bim* will likely have occurred. The role for miR-17~92 miRNAs in *Bim*-dependent endothelial cell death may be stimulus specific, as only a small reduction in death was observed in endothelial cells over-expressing miR-17 in response to H_2O_2 (54). As discussed above, it is possible that FOXO-dependent transcription may mediate the apoptotic response of endothelial cells to oxidative stress and the impact of miR-17 over-expression on serum and growth factor withdrawal was not investigated in that study (54).

Given heterozygous loss of the miR-17~92 cluster did not induce *Bim* to the same extent as serum and growth factor withdrawal, we consider it highly unlikely that it acts alone or is the predominant regulator of *Bim* expression in these cells. The transcription factor E2F1 has been reported to directly induce *Bim* transcription in endothelial cells in response to angiogensin II, and this activity was suppressed by PI3K/Akt (55). E2F1 may therefore be a critical transcriptional inducer of *Bim* following growth factor withdrawal and be a target for Akt-mediated repression of *Bim* transcription in endothelial cells. Interestingly, E2F1 is also a target of the *miR-17~92* cluster (56), and this may provide an additional conduit for *miR17~92*-mediated suppression of *Bim* induction. E2F1 is only one of eight E2F family members (57), therefore discerning its involvement in endothelial apoptosis may be complicated by functional redundancy.

Our results demonstrate a cell-autonomous role of BIM in endothelial cell apoptosis, confirming that the intrinsic apoptotic pathway is active within endothelial cells. This finding supports the likelihood that small molecule death agonists that mimic the activity of BH3-only proteins like BIM (so called 'BH3-mimetics') may be capable of directly targeting endothelial cells and may find use in an anti-angiogenic context.

Materials and Methods

Mice

All experiments involving animals were performed with procedures approved by the Walter and Eliza Hall Institute of Medical Research Animal Ethics Committee. *Bim*$^{-/-}$ (42), *Bim*$^{lacZ/lacZ}$ (32), *Foxo3*$^{-/-}$ (58), *Bim*$^{\Delta Foxo/\Delta Foxo}$ (34), and *miR17~92*$^{fl/+}$ mice (37) have been described previously. Animals were maintained on an inbred C57BL/6 background. *Bim* mutants and littermate controls were generated through heterozygote intercrosses, *Foxo3* mutants and littermate controls were generated through either heterozygote intercross or heterozygote x homozygote intercross. *Bim*$^{\Delta Foxo}$ mutant mice were generated through homozygote intercrosses and compared to age-matched C57BL/6 control mice. *miR17~92*$^{+/-}$ mutants were generated by crossing *miR17~92*$^{fl/+}$ mice with a ubiquitous cre deleter (59), then mutants generated by heterozygote intercross.

Endothelial cell culture and viability assay

E9.5 embryos were dissected free of extra-embryonic membranes. Each embryo was dissociated individually in 1 mL of PBS containing 0.25 WU/mL LiberaseTM (Roche), 10 μg/mL DNaseI and 5 mM $MgCl_2$ for 45 min at 37^{O}C with constant agitation (800 rpm). Dissociated cells were stained using anti-PECAM1-APC (clone 390, eBiosciences), anti-ICAM2-FITC (BD Bioscience), anti-CD41-biotin (clone MWReg30) and anti-CD45.2-biotin (clone S450) antibodies, and streptavidin-PE. Endothelial cells were FACS sorted using an Influx cell sorter (BD Bioscience) and defined as PECAM1^{Hi} ICAM2^{Hi} CD45- CD41- cells. Dead cells were excluded based on DAPI uptake. Endothelial cells were directly deposited into bovine fibronectin-coated (2.5 μg/cm^2) 96 well, optical bottom plates (Nunc). Between 5,700 – 7,000 endothelial cells were plated per well. Cells were cultured for 3 days in complete media (MCDB131 media containing 5% serum, 100 U/mL penicillin, 100 μg/mL streptomycin, 10 mM HEPES, 2 mM glutamax, 5.5 μM 2-mercaptoethanol, 75 μg/mL ascorbic acid, 1 μg/mL hydrocortisone, 10 ng/mL rhVEGF-A, 5 ng/mL rhFGF2, 15 ng/mL rhIGF1 and 5 ng/mL rhEGF) at 37^{O}C in a 5% CO_2 humidified incubator. To assess endothelial purity and viability, unfixed, live cells were incubated for 15 min with biotinylated anti-PECAM1 antibody in complete media under normal culture conditions,

washed and then incubated for 15 min with streptavidin-Alexa Fluor488 in complete media under normal culture conditions. Cells were then deprived of serum and growth factors by rinsing each well twice with MCDB131 media containing 0.1% serum and once with starvation media (complete media containing 0.1% serum and no growth factors). Cells were then cultured in starvation media containing 10 μM MitoTracker Red (Invitrogen) and 0.1 μg/mL DAPI for 1 h prior to initiating time-lapse imaging. This was considered to be t = 0. Time-lapse imaging was performed on a Nikon TiE inverted microscope equipped with a Spot Pursuit cooled CCD camera (Spot Imaging) and operated using MetaMorph software. Images were acquired hourly using a Plan Fluor ELWD 20x/0.45 NA objective (Nikon) for 36 h and binned 2 x 2 to minimize exposure time. Cell number per well was determined by manually counting the number of cells per field of view at t = 0 based on the MitoTracker Red signal. Endothelial purity was determined at t = 0 by determining the number of cells that were positive for PECAM1 in each field of view. As only dying cells take up DAPI in unfixed samples, viability was determined by counting the number of DAPI signals at each time point per field of view using the "count nuclei" function in MetaMorph and expressed as a percentage of the number of viable cells observed in that field of view at t = 0. Viability per well was taken as the average of two randomly selected fields of view. For RNA analysis, endothelial cells were cultured for 24 h with or without serum and growth factors in the presence of 25 μM QVD-OPH caspase inhibitor (MP Biomedicals) to prevent cell death and consequent degradation of proteins and mRNA.

Immunohistochemical analysis of hyaloid and retinal vasculature

Hyaloid vessel dissection and quantitation was performed essentially as described (31). Briefly, eyes were enucleated, fixed in 4% paraformaldehyde for 4 h, injected with 5% gelatin at 40^{o}C then allowed to set at 4^{o}C overnight before dissection and mounting on Polysine coated slides (Thermo Scientific). Hyaloid vessels were stained for PECAM1 (clone MEC13.3, BD Pharmingen), which was detected using fluorescently conjugated anti-rat secondary antibodies (Jackson ImmunoResearch). Vessels were mounted in ProLong Gold antifade reagent containing DAPI (Invitrogen). Terminal deoxynucleotidyl transferase dUTP nick-end labeling (TUNEL) assay was performed using the ApopTag Red *in situ* apoptosis detection kit as per the manufacturer's instructions (Millipore) with the exception

that the reaction was conducted at room temperature for 2 h. Samples were then stained with PECAM1 antibody and DAPI as described above. All hyaloid samples were imaged by wide field microscopy using a Zeiss Axiovert 200M equipped with a Zeiss MRm Axiocam camera, 0.63x C-mount, and either a Zeiss Fluar 5x/0.25 NA or Plan Apochromat 10x/0.45 NA objective. Post-acquisition, tiled images were merged and minor adjustments to brightness and contrast made using ImageJ software. Only non-regressing vessels were considered for quantitation. Regressing vessels were defined based on the presence of TUNEL+ cells, or a discontinuous PECAM1 signal. All hyaloid data are presented as mean ± standard error of the mean with *n* values representing the number of individual animals studied per genotype (a minimum of three eyes were examined for each genotype in each experiment).

For retina analysis, eyes were enucleated and fixed in 4% paraformaldehyde for 2 hours at 4°C. Retinas were then dissected, incubated in blocking buffer (2% normal donkey serum, 1% Triton X-100 in HBSS) then stained with biotinylated isolectin B4 (Vector Laboratories), goat anti-collagen IV antibody (Millipore) and rabbit anti-cleaved (activated) caspase 3 antibody (Cell Signaling Technologies or Promega). Retinas were washed then incubated with secondary antibodies: Streptavidin-Alexa-Fluor488 (Jackson ImmunoResearch), anti-goat IgG Alexa-Fluor 647 (Jackson ImmunoResearch) and anti-rabbit IgG Cy3 (Jackson ImmunoResearch). Retinas were then washed before being mounted on slides in ProLong Gold antifade reagent (Invitrogen). Retinas were imaged using a Zeiss LSM 780 confocal microscope with a 20x/0.8 NA objective. Apoptotic endothelial cells were identified by the presence of a cleaved caspase-3 signal within an Isolectin-B4 positive vessel. Quantification of cleaved caspase-3 positive endothelial cells was performed manually using Image-J.

Expression analysis using sorted hyaloid endothelial cells

Hyaloid vessels were dissociated from P1 or P5 C57BL/6 mice. Vessels from multiple animals at each age were pooled and dissociated in PBS containing 0.25 WU/mL Liberase TM (Roche) and 0.1 μg/mL DNaseI. Dissociated cells were then stained using the following antibodies: anti-PECAM1-APC (clone MEC13.3, BD Bioscience) and anti-Mac1-FITC (clone M1/70). Endothelial cells were FACS sorted as PECAM1+ Mac1- cells that were viable based on propidium iodide exclusion. For QPCR analysis, total RNA from P1

and P5 hyaloid endothelial cells was extracted using Trizol Reagent (Invitrogen) and reverse transcribed using QuantiTect Reverse Transcription Kit (Qiagen) as per the manufacturers instructions. Quantitation of gene expression was performed by real-time polymerase chain reaction (PCR) with 2x SYBR mix (Roche) using a LightCycler 480 (Roche). Each reaction was performed in technical triplicate and expression calculated using the ΔΔct method. Oligonucleotides used were as follows: *Pgk1* (5'-tacctgctggctggatgg and 5'-cacagcctcggcatatttct) and *Bim* (5'-cgtccacccaatgtctgact and 5'-gctgcaattgtccaccttct). Data are presented as mean ± standard error of the mean of three separate cell sorts at P1 and three separate cell sorts at P5. For semi-quantitative RT-PCR, hyaloid endothelial cells from P5 C57BL/6 mice were dissociated essentially as described above. Cells were stained with the following antibodies: anti-PECAM1-APC, anti-CD45.2-FITC (BD Bioscience) and anti-Ter119-PE (BD Pharmingen), then FACS sorted as PECAM1+ CD45.2- Ter119- cells that were viable based on propidium iodide exclusion. RNA was extracted using Trizol Reagent (Invitrogen) and reverse transcribed using Superscript III reverse transcriptase (Invitrogen) and PCR performed on serial 1/5 dilutions of cDNA using the JumpStart REDTaq ReadyMix (Sigma). Oligonucleotide sequences used were as follows: *Foxo1* (5'-aagagcgtgccctacttcaa and 5'-tgctgtgaagggacagattg), *Foxo3* (5'-cttcaaggataagggcgaca and 5'-ctgtgcagggacaggttgt), *Foxo4* (5'-ggtgccctacttcaaggaca and 5'-ctgtgcaaggacaggttgtg) and *Hprt* (5'-gatggccacaggactagaaca and 5'-tccctggttaagcagtacagc).

RNA isolation and qRT-PCR analysis of Bim and microRNA expression

Total RNA was isolated using TRIzol LS (Life Technologies). For analysis of mRNA, 300 ng of total RNA was reverse transcribed using the Superscript III First Strand Synthesis System for RT-PCR (Life Technologies) following the manufacturer's instructions. For quantitative PCR, 1 μL of the cDNA synthesis product was used. For the analysis of micro RNA 10 ng of Trizol isolated RNA was reverse transcribed with micro RNA-specific primers using the TaqMan Micro RNA assay kit (Life Technologies). TaqMan PCR was performed using a mouse *Bim* probe (Life Technologies Cat# MM00437796), a mouse *HMBS* probe (Life Technologies Cat# MM01143545), a U6 snRNA probe (Life Technologies Cat# 001973; 4427975), a miR17-5p probe (Life Technologies Cat# 002308:

4427975) and a miR92a-3p probe (Life Technologies Cat# 000430; 4427975) following the manufacturer's protocols. Data were calculated using the $2^{-\Delta\Delta ct}$ method.

In situ hybridization

Radioactive in situ hybridization was performed in order to locate Bim transcripts essentially as described previously (60). Briefly, eyes from postnatal mice were dissected and fixed in 4% paraformaldehyde then embedded in 1% low melting point agarose and then embedded in paraffin before 8µm sections were cut. To localise *Bim* mRNA sections were dewaxed, rehydrated through graded concentrations of alcohol, and then treated with proteinase K (10µg/mL) for 10 minutes, fixed in 4% paraformaldehyde for a further 10 minutes then dehydrated through a graded alcohol series. Sections were then air-dried. *Bim* sense and antisense cRNA probes were generated by in vitro transcription of a *Bim* cDNA using T3 and T7 RNA polymerases incorporating [^{35}S] labelled nucleotides. After purification cRNA probes were partially hydrolyzed to allow efficient penetration and then incubated overnight at 56°C on the tissue sections. Slides were washed at 65°C including an RNAaseA step to remove single stranded RNA molecules. Finally slides were dipped in liquid film emulsion (Ilford), developed after 1 to 2 weeks at 4°C then counterstained with haematoxylin. Images were acquired on a Zeiss Axioplan 2 microscope equipped with an Axiocam HRc camera using a 10x/0.3 NA Plan Neofluar objective. For clarity, darkfield images were converted to grayscale using Image J software.

Statistical analysis

All statistical analysis was performed using a two-tailed Student's t-test.

Acknowledgements

The authors thank Lachlan Whitehead, Cameron Nowell and Kelly Rogers for expert imaging assistance, Lisa Sampurno for technical assistance, Merle Dayton, Keti Stoev, Chrystal Smith and Emma Lanera for expert animal care and members of the Development and Cancer Division (WEHI) for informative discussion. This work was made possible through Victorian State Government Operational Infrastructure Support and Australian Government NHMRC IRIISS. This work was supported by the National Health and Medical Research Council, Australia (Project Grants: 1010638, 1046010 & 1049720, Program Grants: 1016701, and Fellowships to TT (1003435), AKV (575512) and AS (1020363)) and Leukemia & Lymphoma Society (Special Center of Research 7001-13). LC is supported by an Australian Research Council Future Fellowship (110100891).

Author contributions

M.N.K, E.N, LR, M.J.H, T.T, A.K.V conducted experiments and interpreted data. E.T conducted experiments. P.B generated essential reagents. A.S planned experiments and interpreted data. L.C conceived the study, planned experiments, conducted experiments, interpreted data and wrote the manuscript. All authors proof-read the manuscript.

Conflict of interest statement:

The authors declare no conflict of interest.

References:

1. Carmeliet P. Angiogenesis in life, disease and medicine. Nature. 2005 Dec 15;438(7070):932-6.
2. Coultas L, Chawengsaksophak K, Rossant J. Endothelial cells and VEGF in vascular development. Nature. 2005 Dec 15;438(7070):937-45.
3. Ebos JM, Kerbel RS. Antiangiogenic therapy: impact on invasion, disease progression, and metastasis. Nat Rev Clin Oncol. 2011 Apr;8(4):210-21.
4. Miller JW, Le Couter J, Strauss EC, Ferrara N. Vascular endothelial growth factor a in intraocular vascular disease. Ophthalmology. 2013 Jan;120(1):106-14.
5. Bergers G, Hanahan D. Modes of resistance to anti-angiogenic therapy. Nat Rev Cancer. 2008 Aug;8(8):592-603.
6. Baffert F, Le T, Sennino B, Thurston G, Kuo CJ, Hu-Lowe D, et al. Cellular changes in normal blood capillaries undergoing regression after inhibition of VEGF signaling. Am J Physiol Heart Circ Physiol. 2006 Feb;290(2):H547-59.
7. Lee S, Chen TT, Barber CL, Jordan MC, Murdock J, Desai S, et al. Autocrine VEGF signaling is required for vascular homeostasis. Cell. 2007 Aug 24;130(4):691-703.
8. Huang J, Frischer JS, Serur A, Kadenhe A, Yokoi A, McCrudden KW, et al. Regression of established tumors and metastases by potent vascular endothelial growth factor blockade. Proc Natl Acad Sci U S A. 2003 Jun 24;100(13):7785-90.
9. Naik E, O'Reilly LA, Asselin-Labat ML, Merino D, Lin A, Cook M, et al. Destruction of tumor vasculature and abated tumor growth upon VEGF blockade is driven by proapoptotic protein Bim in endothelial cells. J Exp Med. 2011 Jul 4;208(7):1351-8.
10. Gerber HP, McMurtrey A, Kowalski J, Yan M, Keyt BA, Dixit V, et al. Vascular endothelial growth factor regulates endothelial cell survival through the phosphatidylinositol 3'-kinase/Akt signal transduction pathway. Requirement for Flk-1/KDR activation. J Biol Chem. 1998 Nov 13;273(46):30336-43.
11. Alon T, Hemo I, Itin A, Pe'er J, Stone J, Keshet E. Vascular endothelial growth factor acts as a survival factor for newly formed retinal vessels and has implications for retinopathy of prematurity. Nature medicine. 1995 Oct;1(10):1024-8.
12. Strasser A, Cory S, Adams JM. Deciphering the rules of programmed cell death to improve therapy of cancer and other diseases. EMBO J. 2011 Sep 14;30(18):3667-83.
13. Gerber HP, Dixit V, Ferrara N. Vascular endothelial growth factor induces expression of the antiapoptotic proteins Bcl-2 and A1 in vascular endothelial cells. J Biol Chem. 1998 May 22;273(21):13313-6.
14. Nor JE, Christensen J, Mooney DJ, Polverini PJ. Vascular endothelial growth factor (VEGF)-mediated angiogenesis is associated with enhanced endothelial cell survival and induction of Bcl-2 expression. Am J Pathol. 1999 Feb;154(2):375-84.
15. Wang S, Sorenson CM, Sheibani N. Attenuation of retinal vascular development and neovascularization during oxygen-induced ischemic retinopathy in Bcl-2-/- mice. Developmental biology. 2005 Mar 1;279(1):205-19.
16. Hahn P, Lindsten T, Tolentino M, Thompson CB, Bennett J, Dunaief JL. Persistent fetal ocular vasculature in mice deficient in bax and bak. Arch Ophthalmol. 2005 Jun;123(6):797-802.
17. Wang S, Park S, Fei P, Sorenson CM. Bim is responsible for the inherent sensitivity of the developing retinal vasculature to hyperoxia. Developmental biology. 2011 Jan 15;349(2):296-309.

18. Youle RJ, Strasser A. The BCL-2 protein family: opposing activities that mediate cell death. Nature reviews Molecular cell biology. 2008 Jan 1;9(1):47-59.
19. Kim I, Kim HG, So JN, Kim JH, Kwak HJ, Koh GY. Angiopoietin-1 regulates endothelial cell survival through the phosphatidylinositol 3'-Kinase/Akt signal transduction pathway. Circ Res. 2000 Jan 7-21;86(1):24-9.
20. Dimmeler S, Assmus B, Hermann C, Haendeler J, Zeiher AM. Fluid shear stress stimulates phosphorylation of Akt in human endothelial cells: involvement in suppression of apoptosis. Circ Res. 1998 Aug 10;83(3):334-41.
21. Fu Z, Tindall DJ. FOXOs, cancer and regulation of apoptosis. Oncogene. 2008 Apr 7;27(16):2312-9.
22. Dijkers PF, Medema RH, Lammers JW, Koenderman L, Coffer PJ. Expression of the pro-apoptotic Bcl-2 family member Bim is regulated by the forkhead transcription factor FKHR-L1. Curr Biol. 2000 Oct 5;10(19):1201-4.
23. Moller C, Alfredsson J, Engstrom M, Wootz H, Xiang Z, Lennartsson J, et al. Stem cell factor promotes mast cell survival via inactivation of FOXO3a-mediated transcriptional induction and MEK-regulated phosphorylation of the proapoptotic protein Bim. Blood. 2005 Aug 15;106(4):1330-6.
24. Gilley J, Coffer PJ, Ham J. FOXO transcription factors directly activate bim gene expression and promote apoptosis in sympathetic neurons. J Cell Biol. 2003 Aug 18;162(4):613-22.
25. Stahl M, Dijkers PF, Kops GJ, Lens SM, Coffer PJ, Burgering BM, et al. The forkhead transcription factor FoxO regulates transcription of p27Kip1 and Bim in response to IL-2. J Immunol. 2002 May 15;168(10):5024-31.
26. Abid MR, Guo S, Minami T, Spokes KC, Ueki K, Skurk C, et al. Vascular endothelial growth factor activates PI3K/Akt/forkhead signaling in endothelial cells. Arteriosclerosis, thrombosis, and vascular biology. 2004 Feb 1;24(2):294-300.
27. Potente M, Urbich C, Sasaki K, Hofmann WK, Heeschen C, Aicher A, et al. Involvement of Foxo transcription factors in angiogenesis and postnatal neovascularization. J Clin Invest. 2005 Sep;115(9):2382-92.
28. Daly C, Wong V, Burova E, Wei Y, Zabski S, Griffiths J, et al. Angiopoietin-1 modulates endothelial cell function and gene expression via the transcription factor FKHR (FOXO1). Genes & development. 2004 May 1;18(9):1060-71.
29. Czymai T, Viemann D, Sticht C, Molema G, Goebeler M, Schmidt M. FOXO3 modulates endothelial gene expression and function by classical and alternative mechanisms. J Biol Chem. 2010 Feb 1.
30. Rao S, Lobov IB, Vallance JE, Tsujikawa K, Shiojima I, Akunuru S, et al. Obligatory participation of macrophages in an angiopoietin 2-mediated cell death switch. Development. 2007 Dec 1;134(24):4449-58.
31. Lobov IB, Rao S, Carroll TJ, Vallance JE, Ito M, Ondr JK, et al. WNT7b mediates macrophage-induced programmed cell death in patterning of the vasculature. Nature. 2005 Sep 15;437(7057):417-21.
32. Bouillet P, Cory S, Zhang LC, Strasser A, Adams JM. Degenerative disorders caused by Bcl-2 deficiency prevented by loss of its BH3-only antagonist Bim. Developmental cell. 2001 Nov;1(5):645-53.
33. Furuyama T, Nakazawa T, Nakano I, Mori N. Identification of the differential distribution patterns of mRNAs and consensus binding sequences for mouse DAF-16 homologues. The Biochemical journal. 2000 Jul 15;349(Pt 2):629-34.

34. Herold MJ, Rohrbeck L, Lang MJ, Grumont R, Gerondakis S, Tai L, et al. Foxo-mediated Bim transcription is dispensable for the apoptosis of hematopoietic cells that is mediated by this BH3-only protein. EMBO reports. 2013 Sep 24.
35. Simonavicius N, Ashenden M, van Weverwijk A, Lax S, Huso DL, Buckley CD, et al. Pericytes promote selective vessel regression to regulate vascular patterning. Blood. 2012 Aug 16;120(7):1516-27.
36. Claxton S, Fruttiger M. Role of arteries in oxygen induced vaso-obliteration. Exp Eye Res. 2003 Sep;77(3):305-11.
37. Ventura A, Young AG, Winslow MM, Lintault L, Meissner A, Erkeland SJ, et al. Targeted deletion reveals essential and overlapping functions of the miR-17 through 92 family of miRNA clusters. Cell. 2008 Mar 7;132(5):875-86.
38. Xiao C, Srinivasan L, Calado DP, Patterson HC, Zhang B, Wang J, et al. Lymphoproliferative disease and autoimmunity in mice with increased miR-17-92 expression in lymphocytes. Nature immunology. 2008 Apr;9(4):405-14.
39. Koralov SB, Muljo SA, Galler GR, Krek A, Chakraborty T, Kanellopoulou C, et al. Dicer ablation affects antibody diversity and cell survival in the B lymphocyte lineage. Cell. 2008 Mar 7;132(5):860-74.
40. Gaengel K, Genove G, Armulik A, Betsholtz C. Endothelial-mural cell signaling in vascular development and angiogenesis. Arteriosclerosis, thrombosis, and vascular biology. 2009 May;29(5):630-8.
41. Franco M, Roswall P, Cortez E, Hanahan D, Pietras K. Pericytes promote endothelial cell survival through induction of autocrine VEGF-A signaling and Bcl-w expression. Blood. 2011 Sep 8;118(10):2906-17.
42. Bouillet P, Metcalf D, Huang DC, Tarlinton DM, Kay TW, Kontgen F, et al. Proapoptotic Bcl-2 relative Bim required for certain apoptotic responses, leukocyte homeostasis, and to preclude autoimmunity. Science. 1999 Nov 26;286(5445):1735-8.
43. Lugus JJ, Park C, Ma YD, Choi K. Both primitive and definitive blood cells are derived from Flk-1+ mesoderm. Blood. 2009 Jan 15;113(3):563-6.
44. Chen MJ, Yokomizo T, Zeigler BM, Dzierzak E, Speck NA. Runx1 is required for the endothelial to haematopoietic cell transition but not thereafter. Nature. 2009 Feb 12;457(7231):887-91.
45. Sheibani N, Morrison ME, Gurel Z, Park S, Sorenson CM. BIM deficiency differentially impacts the function of kidney endothelial and epithelial cells through modulation of their local microenvironment. American journal of physiology Renal physiology. 2012 Apr 1;302(7):F809-19.
46. Coultas L, Bouillet P, Stanley EG, Brodnicki TC, Adams JM, Strasser A. Proapoptotic BH3-only Bcl-2 family member Bik/Blk/Nbk is expressed in hemopoietic and endothelial cells but is redundant for their programmed death. Mol Cell Biol. 2004 Feb;24(4):1570-81.
47. Zhang F, Li Y, Tang Z, Kumar A, Lee C, Zhang L, et al. Proliferative and survival effects of PUMA promote angiogenesis. Cell reports. 2012 Nov 29;2(5):1272-85.
48. Villunger A, Michalak EM, Coultas L, Mullauer F, Bock G, Ausserlechner MJ, et al. p53- and drug-induced apoptotic responses mediated by BH3-only proteins puma and noxa. Science. 2003 Nov 7;302(5647):1036-8.
49. Coultas L, Bouillet P, Loveland KL, Meachem S, Perlman H, Adams JM, et al. Concomitant loss of proapoptotic BH3-only Bcl-2 antagonists Bik and Bim arrests spermatogenesis. Embo J. 2005 Nov 16;24(22):3963-73.

50. Urbich C, Knau A, Fichtlscherer S, Walter DH, Bruhl T, Potente M, et al. FOXO-dependent expression of the proapoptotic protein Bim: pivotal role for apoptosis signaling in endothelial progenitor cells. FASEB journal : official publication of the Federation of American Societies for Experimental Biology. 2005 Jun;19(8):974-6.
51. Shen B, Gao L, Hsu YT, Bledsoe G, Hagiwara M, Chao L, et al. Kallistatin attenuates endothelial apoptosis through inhibition of oxidative stress and activation of Akt-eNOS signaling. Am J Physiol Heart Circ Physiol. 2010 Nov;299(5):H1419-27.
52. Huntzinger E, Izaurralde E. Gene silencing by microRNAs: contributions of translational repression and mRNA decay. Nature reviews Genetics. 2011 Feb;12(2):99-110.
53. Suarez Y, Fernandez-Hernando C, Yu J, Gerber SA, Harrison KD, Pober JS, et al. Dicer-dependent endothelial microRNAs are necessary for postnatal angiogenesis. Proc Natl Acad Sci U S A. 2008 Sep 16;105(37):14082-7.
54. Doebele C, Bonauer A, Fischer A, Scholz A, Reiss Y, Urbich C, et al. Members of the microRNA-17-92 cluster exhibit a cell-intrinsic antiangiogenic function in endothelial cells. Blood. 2010 Jun 10;115(23):4944-50.
55. Kim YC, Day RM. Angiotensin II regulates activation of Bim via Rb/E2F1 during apoptosis: involvement of interaction between AMPKbeta1/2 and Cdk4. Am J Physiol Lung Cell Mol Physiol. 2012 Aug 1;303(3):L228-38.
56. O'Donnell KA, Wentzel EA, Zeller KI, Dang CV, Mendell JT. c-Myc-regulated microRNAs modulate E2F1 expression. Nature. 2005 Jun 9;435(7043):839-43.
57. Biswas AK, Johnson DG. Transcriptional and nontranscriptional functions of E2F1 in response to DNA damage. Cancer Res. 2012 Jan 1;72(1):13-7.
58. Miyamoto K, Araki KY, Naka K, Arai F, Takubo K, Yamazaki S, et al. Foxo3a is essential for maintenance of the hematopoietic stem cell pool. Cell stem cell. 2007 Jun 7;1(1):101-12.
59. Schwenk F, Baron U, Rajewsky K. A cre-transgenic mouse strain for the ubiquitous deletion of loxP-flanked gene segments including deletion in germ cells. Nucleic acids research. 1995 Dec 25;23(24):5080-1.
60. Thomas T, Voss AK, Chowdhury K, Gruss P. Querkopf, a MYST family histone acetyltransferase, is required for normal cerebral cortex development. Development. 2000 Jun;127(12):2537-48.

Titles and Legends to Figures

Figure 1. BIM is autonomously required for endothelial cell apoptosis in response to serum and growth factor withdrawal. (**a**) Endothelial cells sorted from E9.5 embryos, cultured for 3 days then stained for PECAM1 (green) and MitoTracker Red (red) (upper panel). Lower panel shows MitoTracker Red signal alone. Shown are representative images of cultures from $Bim^{+/+}$, $Bim^{+/-}$ and $Bim^{-/-}$ embryos. The total number of cells was counted in each field based on MitoTracker signal and endothelial cells identified as $PECAM1^{+}$ $MitoTracker\ Red^{+}$. Arrows indicate cells that were negative for PECAM1. Scale bar = 200 μm. (**b**) Time course of endothelial cell death following serum and growth factor withdrawal. Loss of viability was determined by counting the number of cells that became permeable to DAPI every hour for 36 h by time-lapse imaging and expressing this as a percentage of the number of viable cells observed at t = 0. Viability was determined for $Bim^{+/+}$ (n = 2 embryos), $Bim^{+/-}$ (n = 4 embryos) and $Bim^{-/-}$ (n = 3 embryos) littermates (*$p<0.05$, $Bim^{-/-}$ vs $Bim^{+/+}$, **$p<0.05$ $Bim^{-/-}$ vs $Bim^{+/-}$, Student's t test). Data are presented as mean ± SEM.

Figure 2. *Bim* is expressed in hyaloid endothelial cells. (**a**) *In situ* hybridization analysis of *Bim* expression in eyes of P6 WT C57BL/6 mice. Left panel shows brightfield image, right panel shows darkfield image. Arrows indicate representative examples of blood vessels labelling positive for the *Bim* probe. L, lens. R, retina. Scale bar = 200 μm. (**b**) Analysis of *Bim* expression by staining for β-galactosidase activity in P7 eyes from $Bim^{lacZ/+}$ mice. Representative images from $Bim^{lacZ/+}$ (n = 2) and littermate $Bim^{+/+}$ (n = 3) mice are shown. Arrows and arrowheads indicate representative examples of macrophages and pericytes respectively. Scale bar = 50 μm.

Figure 3. BIM is required for hyaloid blood vessel regression. (**a**) Hyaloid vessel number was quantified in eyes from $Bim^{-/-}$ (n = 4) and $Bim^{+/+}$ (n = 3) littermates at P8. DAPI images of representative hyaloid membrane whole mount spread preparations from $Bim^{-/-}$ and $Bim^{+/+}$ mice are shown. $Bim^{-/-}$ mice had significantly more vessels per eye than littermates (*p = 0.018, Student's t-test). Data are presented as mean ± SEM. (**b**) Representative image of a hyaloid vessel whole mount from a P8 $Bim^{-/-}$ pup (n = 5), stained by TUNEL DNA

fragmentation assay (red) and for the endothelial marker PECAM1 (grey). Arrows demarcate TUNEL^{+} vessels undergoing synchronous apoptosis and vessel regression. (**c**) Representative images of eyes from *Bim*$^{-/-}$ and WT adult eyes. Arrows indicate persisting hyaloid vessels.

Figure 4. BIM-dependent hyaloid vessel regression occurs independently of FOXO regulation. (**a**) *Bim* mRNA levels in P1 and P5 hyaloid endothelial cells determined by quantitative RT-PCR. *Bim* levels were normalized to *Pgk1* and expressed as fold change relative to P1. Data are presented as mean ± SEM from 3 independent mRNA preparations at both P1 and P5. (**b**) Hyaloid vessel number was quantified in eyes from *Foxo3*$^{+/+}$ (n = 4) and *Foxo3*$^{-/-}$ (n = 4) littermates at P8. Data are presented as mean ± SEM. (**c**) Semi-quantitative RT-PCR analysis of *Foxo1*, *Foxo3* and *Foxo4* mRNA levels in FACS sorted P5 hyaloid endothelial cells. *Hprt* is included as a loading control. Negative (water) and positive controls for each gene are included. (**d**) Hyaloid vessel number was quantified in eyes from *Bim*$^{\Delta Foxo/\Delta Foxo}$ (n = 4) and WT (n = 4) mice at P8. Data are presented as mean ± SEM.

Figure 5. BIM-dependent endothelial apoptosis during hypoxia-driven angiogenesis occurs independently of FOXO regulation. (**a**) Quantitative analysis of apoptotic endothelial cells in retinas of *Bim* mutants at P5 by immunohistochemical detection of active caspase-3. Representative confocal immunofluorescence microscopy images from *Bim*$^{+/-}$ and *Bim*$^{-/-}$ retina whole mounts are shown. Apoptotic cells were detected by staining for active caspase-3 (red) and endothelial cells using isolectinB4 (grey). The total number of apoptotic endothelial cells per retina was determined from control genotypes (combined *Bim*$^{+/+}$ and *Bim*$^{+/-}$) (n = 3) and *Bim*$^{-/-}$ (n = 3) littermates. Data are presented as mean ± SEM (*p = 0.016, Student's t-test). Arrows indicate apoptotic endothelial cells. Scale bar = 50 μm. (**b**) Quantitative analysis of apoptotic endothelial cells in retinas of *Foxo3* mutants at P5, as described in *(a)*. The total number of apoptotic endothelial cells per retina was determined from *Foxo3*$^{+/-}$ (n = 4) and *Foxo3*$^{-/-}$ (n = 4) littermates. (**c**) Quantitative analysis of apoptotic endothelial cells in retinas of *Bim*$^{\Delta Foxo/\Delta Foxo}$ mutants at P5, as described in *(a)*. The total number of apoptotic endothelial cells per retina was determined from WT (n = 3) and *Bim*$^{\Delta Foxo/\Delta Foxo}$ (n = 4) animals. Data are presented as mean ± SEM.

Figure 6. *Bim* mRNA induction in serum and growth factor starved endothelial cells is accompanied by reduction in *miR-17~92* cluster miRNAs. (**a**) Quantitative RT-PCR analysis of *Bim* in endothelial cells grown in the presence (unstarved) or absence (starved) of serum and growth factors for 24 h. Caspase inhibitor QVD-OPH was added to all cultures to prevent loss of cells undergoing apoptosis. Expression of *Bim* mRNA was normalized to *hmbs*. Data are represented as fold change relative to unstarved and presented as mean ± standard deviation of two independent experiments (3 replicates per experiment). (**b**) Quantitative RT-PCR analysis of miR-17-5p and miR-92a-3p in 24 h unstarved and starved endothelial cells as described in *(a)*. **(c)** Quantitative RT-PCR analysis of *Bim* in *mir-17~92* control genotypes (controls) and *mir-17~92*$^{+/-}$ endothelial cells. Cells were grown in the presence (unstarved) or absence (starved) of serum and growth factors for 24 h along with QVD-OPH caspase inhibitor to prevent loss of cells that have initiated apoptosis. Data are represented as fold change relative to unstarved *mir-17~92* control genotypes and presented as mean ± SEM. (*p = 0.013, *ns* = not significant, Student's t-test). Cells from individual embryos were used to generate data for each genotype and condition: *mir-17~92* control unstarved (n = 3 embryos), *mir-17~92*$^{+/-}$ unstarved (n = 3 embryos), *mir-17~92* control starved (n = 6 embryos), *mir-17~92*$^{+/-}$ starved (n = 3 embryos).

Figure 1

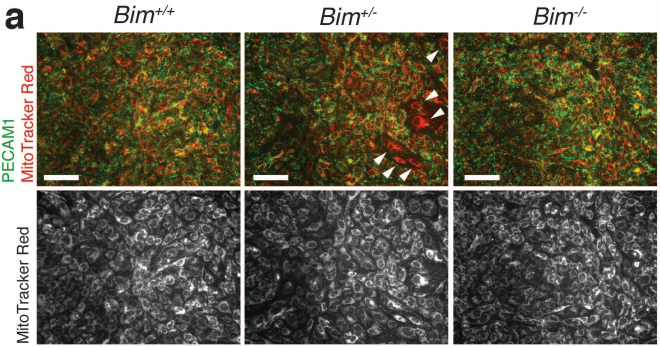
a
Bim+/+
Bim+/-
Bim-/-
PECAM1
MitoTracker Red
MitoTracker Red

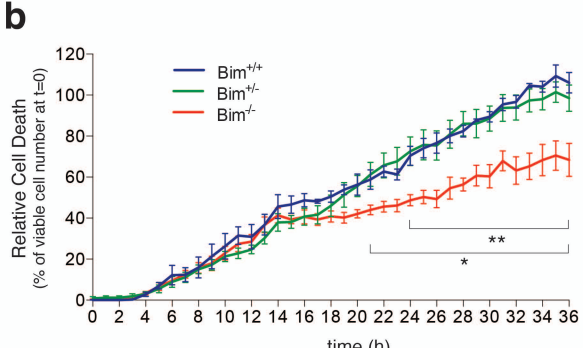
b
Relative Cell Death
(% of viable cell number at t=0)
Bim+/+
Bim+/-
Bim-/-
**
*
time (h)

Figure 2

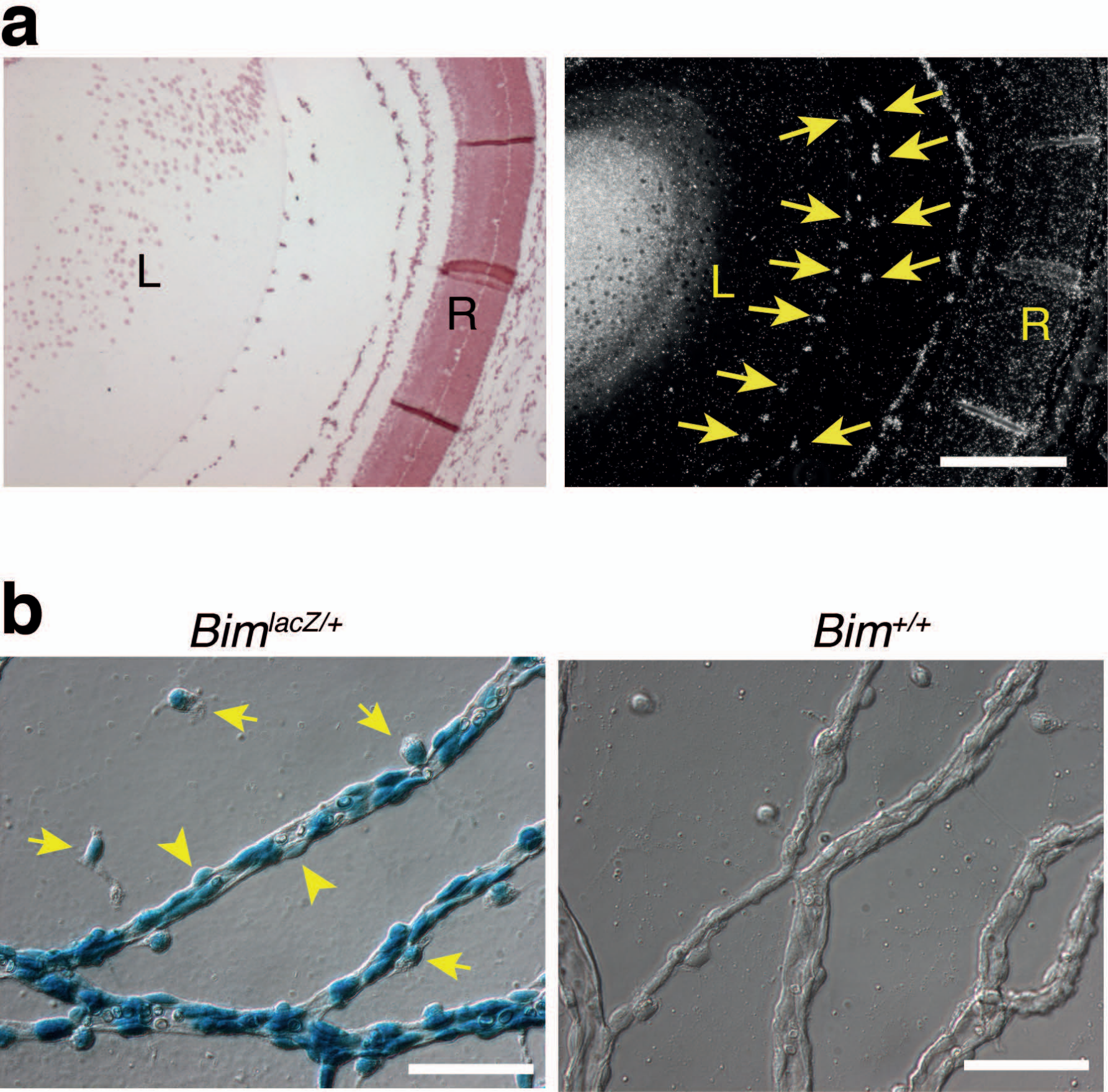

Figure 3

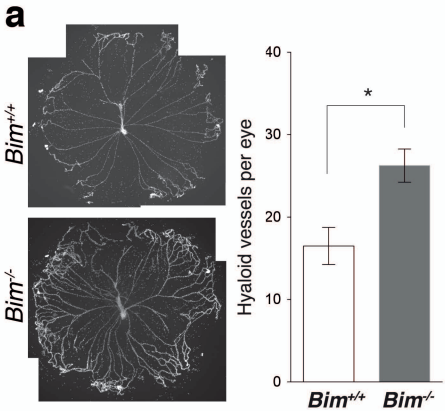

Figure 4

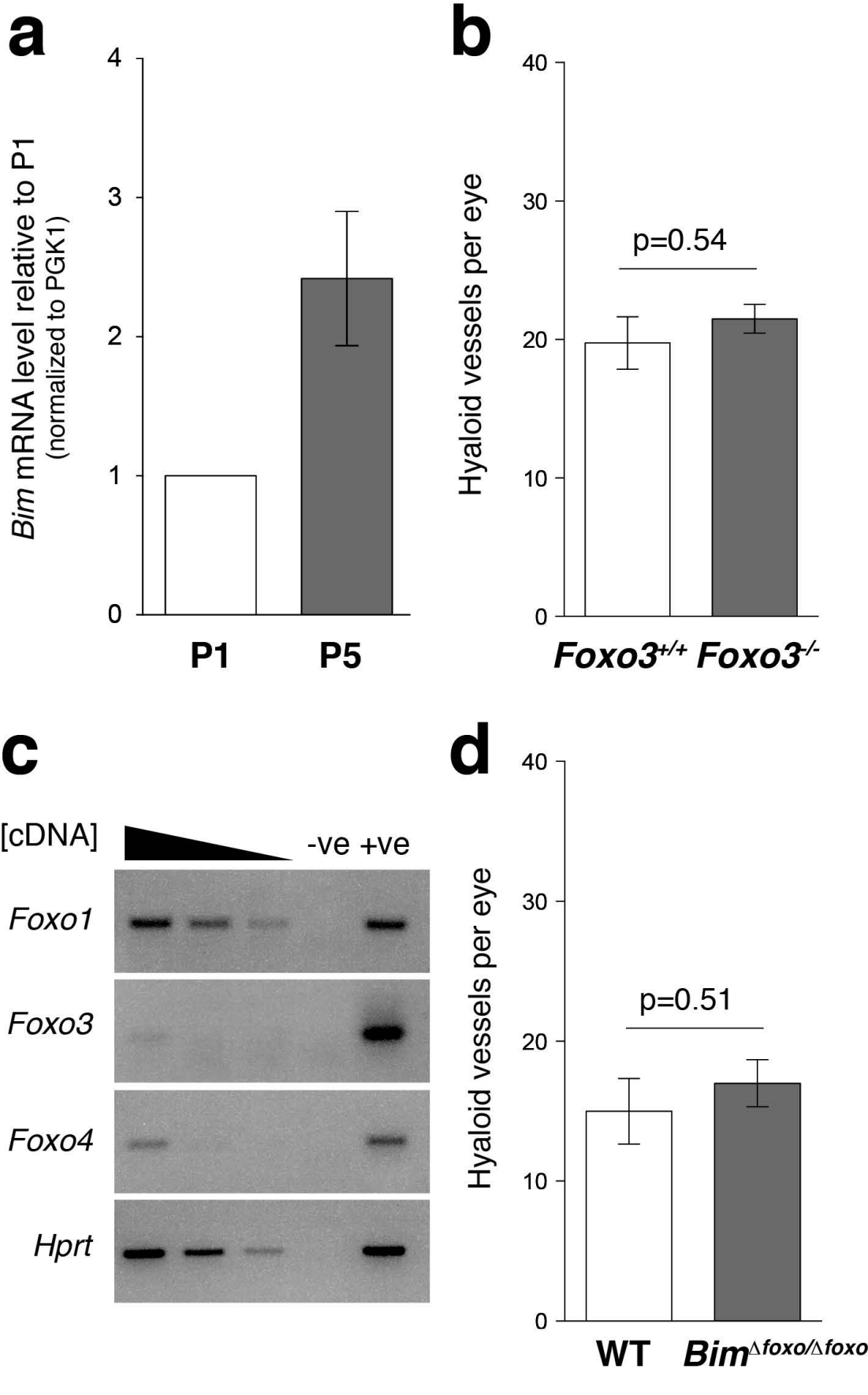
a
Bim mRNA level relative to P1
(normalized to PGK1)
4
3
2
1
0
P1
P5
b
Hyaloid vessels per eye
40
30
20
10
0
p=0.54
Foxo3+/+
Foxo3-/-
c
[cDNA]
-ve +ve
Foxo1
Foxo3
Foxo4
Hprt
d
Hyaloid vessels per eye
40
30
20
10
0
p=0.51
WT
Bim∆foxo/∆foxo

Figure 5

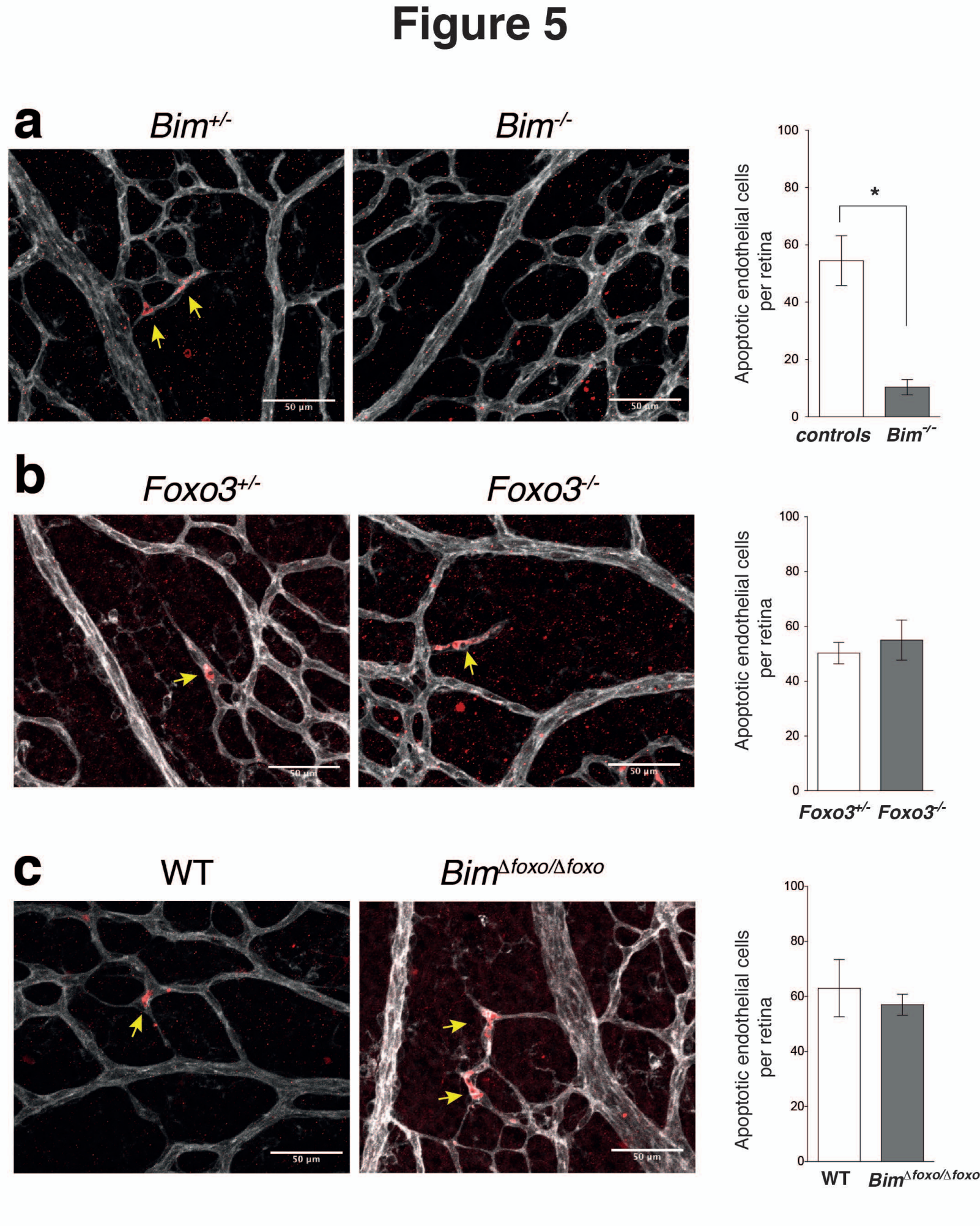
a
Bim+/-
Bim-/-
50 µm
50 µm
Apoptotic endothelial cells per retina
100
80
60
40
20
0
*
controls
Bim-/-
b
Foxo3+/-
Foxo3-/-
50 µm
50 µm
Apoptotic endothelial cells per retina
100
80
60
40
20
0
Foxo3+/-
Foxo3-/-
c
WT
BimΔfoxo/Δfoxo
50 µm
50 µm
Apoptotic endothelial cells per retina
100
80
60
40
20
0
WT
BimΔfoxo/Δfoxo

Figure 6

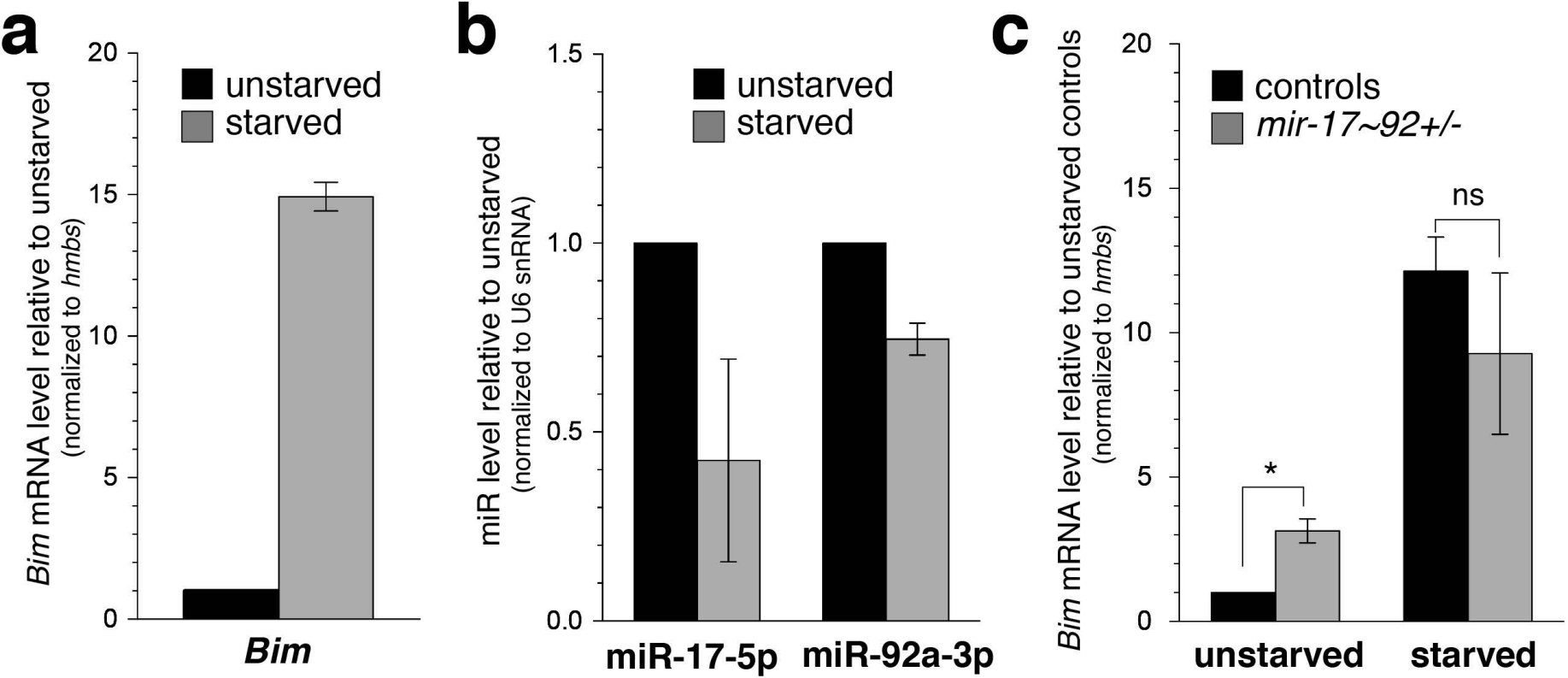
a
Bim mRNA level relative to unstarved
(normalized to hmbs)
20
15
10
5
0
unstarved
starved
Bim
b
miR level relative to unstarved
(normalized to U6 snRNA)
1.5
1.0
0.5
0.0
unstarved
starved
miR-17-5p
miR-92a-3p
c
Bim mRNA level relative to unstarved controls
(normalized to hmbs)
20
15
10
5
0
controls
mir-17~92+/-
ns
*
unstarved
starved